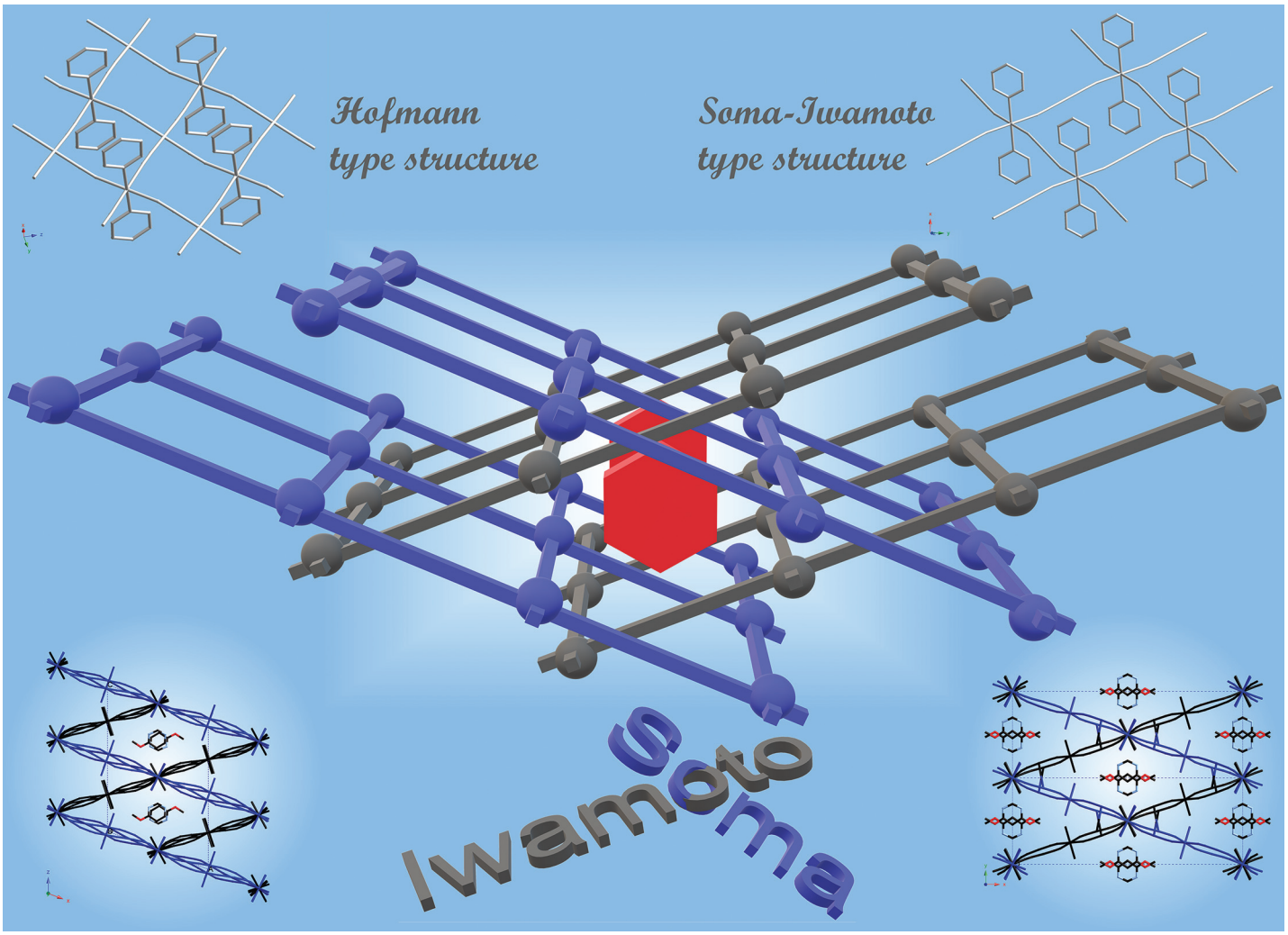

Showcasing research from Professor Kitazawa's laboratory, Department of Chemistry, Toho University, Chiba, Japan.

Guest-triggered "Soma–Iwamoto-type" penetration complex {Fe(4-ethoxypyrimidine)$_2$[M(CN)$_2$]$_2$}·Guest (M = Ag, Au)

Many laboratories perform extensive studies on the spin-crossover (SCO) phenomenon. Currently, we have synthesized novel "Soma–Iwamoto type" complexes that contain 4-methoxypyrimidine (4-MeOPmd) ligand, {Fe(4-MeOPmd)$_2$[Ag(CN)$_2$]$_2$}, {Fe(4-MeOPmd)$_2$[Au(CN)$_2$]$_2$}, and {Fe(4-MeOPmd)$_2$[Ag(CN)$_2$]$_2$·0.25(4-MeOPmd)}. Moreover, we synthesized 4,6-dimethoxypyrimidine (4,6-diMeOPmd) clathrate complex, *i.e.* {Fe(4-MeOPmd)$_2$[Ag(CN)$_2$]$_2$·0.25(4,6-diMeOPmd)} and {Fe(4-MeOPmd)$_2$[Au(CN)$_2$]$_2$·0.25(4,6-diMeOPmd)}. The guest clathrate complexes demonstrate the SCO phenomenon and interesting rarely reported penetrated structures with two Soma–Iwamoto-type structures.

As featured in:

See Takafumi Kitazawa *et al.*, *Dalton Trans.*, 2023, **52**, 2571.

ROYAL SOCIETY OF CHEMISTRY

rsc.li/dalton

Registered charity number: 207890

Dalton Transactions

ROYAL SOCIETY OF CHEMISTRY

PAPER

View Article Online
View Journal | View Issue

Check for updates

Cite this: *Dalton Trans.*, 2023, **52**, 2571

Guest-triggered "Soma–Iwamoto-type" penetration complex {Fe(4-methoxypyrimidine)$_2$[M(CN)$_2$]$_2$}·Guest (M = Ag, Au)†

Kosuke Kitase, [a] Daisuke Akahoshi[b] and Takafumi Kitazawa*[a,c]

Received 18th November 2022,
Accepted 23rd January 2023

DOI: 10.1039/d2dt03716e

rsc.li/dalton

Many laboratories have performed extensive studies on the spin-crossover (SCO) phenomenon. Herein, we synthesized novel "Soma–Iwamoto type" complexes containing a 4-methoxypyrimidine (4-MeOPmd) ligand, *i.e.*, {Fe(4-MeOPmd)$_2$[Ag(CN)$_2$]$_2$} (**1Ag**), {Fe(4-MeOPmd)$_2$[Au(CN)$_2$]$_2$} (**1Au**), and {Fe(4-MeOPmd)$_2$[Ag(CN)$_2$]$_2$·0.25(4-MeOPmd)} (**1Ag·0.25G**). Moreover, we synthesized a 4,6-dimethoxypyrimidine (4,6-diMeOPmd) clathrate complex, *i.e.*, {Fe(4-MeOPmd)$_2$[Ag(CN)$_2$]$_2$·0.25(4,6-diMeOPmd)} (**2Ag·0.25G**) and {Fe(4-MeOPmd)$_2$[Au(CN)$_2$]$_2$·0.25(4,6-diMeOPmd)} (**2Au·0.25G**). Some of these complexes, *i.e.*, **1Ag·0.25G**, **2Ag·0.25G**, and **2Au·0.25G**, demonstrated penetrated structures, which are very interesting given that they have rarely been reported to date. **1Au** and **1Ag** did not show the SCO phenomenon, **1Ag·0.25G** showed a gradual multi-step SCO phenomenon, and **2Au·0.25G** and **2Ag·0.25G** showed an abrupt half SCO phenomenon.

Introduction

The spin-crossover (SCO) phenomenon is a reversible spin transition between high-spin (HS) and low-spin (LS) states in response to heat, pressure, or light. Recently, many groups have investigated SCO because of the potential of functional materials for applications such as molecular machines, data storage devices, switching devices, and sensors. Moreover, a Hofmann-type structure is a coordination polymer that contains a center metal ion, bridging cyanometalate ligand, and pillar ligands such as pyridine and pyrazine. The first Hofmann-type complex, $Ni(NH_3)_2[Ni(CN)_4]\cdot 2(C_6H_6)$, was reported by K. A. Hofmann.[1] Alternatively, the first Hofmann-type SCO complex, $Fe(Py)_2[Ni(CN)_4]$, was reported by Kitazawa *et al.*[2] Subsequently, many laboratories have investigated Hofmann-type complexes because of their tunable properties. To date, the reported "Hofmann-type" complexes can be divided into two types. The first type is bridged by square planar tetra-coordinated divalent cyanometalate $[M(CN)_4]^{2-}$ (M = Ni, Pd, Pt)[3–10] such as $Fe(pz)[M(CN)_4]\cdot H_2O$ (M = Ni, Pd, Pt),[10] while the other is bridged by linear coordinated monovalent cyanometalate $[M(CN)_2]^-$ (M = Ag, Au).[11–16] The first complex possessing the latter type of structure is $[Cd(4,4'\text{-bpy})_2\{Ag(CN)_2\}_2]$,[17] while the second is $[Cd(py)_2\{Ag(CN)_2\}_2]$,[18,19] which were both reported by Soma and Iwamoto, and therefore, the latter type of structures are denoted as "Soma–Iwamoto types". Coordination polymer frameworks of Hofmann-type $ML_2M'(CN)_4$ (M′ = Ni, Pd, Pt) structures are different from that of the Soma–Iwamoto type $ML_2[M''(CN)_2]_2$ (M″ = Ag, Au). The mesh size of the Soma–Iwamoto-type structure is about four-times larger than the Hofmann-type structure because the side length of the former is approximately twice as long as that of the latter. Soma–Iwamoto type Fe complexes were also previously reported, where first reported one was $Fe(py)_2\{Au(CN)_2\}_2$[20] and $Fe(py)_2\{Ag(CN)_2\}_2$.[21]

However, although many Hofmann-type and Soma–Iwamoto-type complexes have been reported, the pillar ligands in most of these complexes belong to pyridine, pyrazine, or bipyridine-type ligands, and only a few of Soma–Iwamoto-type complexes using pyrimidine-type ligands as a pillar ligand have been reported.

Previously, we reported the preparation of two Soma–Iwamoto-type SCO complexes, $\{Fe(4\text{-methylpyrimidine})_2[Au(CN)_2]_2\}$[15] and $\{Fe(4\text{-methylpyrimidine})_2[Ag(CN)_2]_2\}$,[16] using 4-methylpyrimidine. These complexes show "normal" stacking of Soma–Iwamoto-type single or double-layer and Soma–

[a]*Department of Chemistry, Toho University, Chiba 274-8510, Japan. E-mail: kitazawa@chem.sci.toho-u.ac.jp*
[b]*Department of Physics, Toho University, Chiba 274-8510, Japan*
[c]*Research Centre for Materials with Integrated Properties, Toho University, Chiba 274-8510, Japan*

†Electronic supplementary information (ESI) available. CCDC 2191439–2191451. For ESI and crystallographic data in CIF or other electronic format see DOI: https://doi.org/10.1039/d2dt03716e

Iwamoto type-structure, where the unique stacking of the Soma–Iwamoto-type layer has not been obtained in pyrimidine-type complexes to date. The interaction between the Ag atom in the bridging ligand and lone pair of the N atom in the 4-methylpyrimidine ligand was observed in {Fe(4-methylpyrimidine)$_2$[Ag(CN)$_2$]$_2$}. In this study, the methyl group in the pyrimidine-type ligand is replaced with a methoxy group, causing additional M–ligand interaction due to the lone pair in the O atom. Thus, we improved the subtle interactions between the cyano-coordinate framework and pyrimidine-type molecule as a second bond, which is associated with spin transition behavior.

Herein, we synthesized novel Soma–Iwamoto type SCO complexes using the 4-methoxypyrimidine ligand, including {Fe(4-methoxypyrimidine)$_2$[Ag(CN)$_2$]$_2$} (**1Ag**), {Fe(4-methoxypyrimidine)$_2$[Au(CN)$_2$]$_2$} (**1Au**), and {Fe(4-methoxypyrimidine)$_2$[Ag(CN)$_2$]$_2$·0.25(4-methoxypyrimidine)} (**1Ag·0.25G**). We also used 4,6-dimethoxypyrimidine as a guest. The reason why this molecule has a similar structure to 4-methoxypyrimidine but cannot coordinate to the Fe center is due to the steric hindrance of both nitrogen atoms in the pyrimidine ring, and consequently this molecule can only act as a guest molecule. Furthermore, we synthesized two complexes, *i.e.*, {Fe(4-methoxypyrimidine)$_2$[Ag(CN)$_2$]$_2$·0.25(4,6-dimethoxypyrimidine)} (**2Ag·0.25G**) and {Fe(4-methoxypyrimidine)$_2$[Au(CN)$_2$]$_2$·0.25(4,6-dimethoxypyrimidine)} (**2Au·0.25G**), using this molecule.

Experimental

The complexes were synthesized using Mohr's salt and cyanometalate.

Mohr's salt was purchased from Kanto Chemical Co., L-ascorbic acid was purchased from Nacalai Tesque Co., K[Au(CN)$_2$] was purchased from Toyo Chemical Industrial Co., and 4-methoxypyrimidine and 4,6-dimethoxypyrimidine were purchased from TCI.

The Fe–Ag Soma–Iwamoto-type complexes (**1Ag**, **1Ag·0.25G**, **2Ag·0.25G**) and Fe–Au Soma–Iwamoto-type complexes (**1Au**, **2Au·0.25G**) were synthesized *via* a direct method and vapor diffusion method, respectively.

Complex **1Au** was synthesized using Mohr's salt Fe(NH$_4$)$_2$(SO$_4$)$_2$·6H$_2$O, L-ascorbic acid and K[Au(CN)$_2$] in a 1 : 1 : 2 molar ratio, and 4-methoxypyrimidine. In the synthesis of the powder sample, 0.3 mmol of Mohr's salt (0.1194 g), 0.28 mmol of L-ascorbic acid (0.0493 g) and 0.6 mmol of K[Au(CN)$_2$] (0.1740 g) were dissolved in 10 mL of water. Then excess 4-methoxypyrimidine (0.3302 g, 3.0 mmol) was dropped into this solution. Subsequently, 0.1522 g (0.196 mmol, 64% yield) of white powder was obtained by this method. In the synthesis of a single crystal, 0.1 mmol of Mohr's salt Fe(NH$_4$)$_2$(SO$_4$)$_2$·6H$_2$O (0.0392 g), 0.1 mmol of L-ascorbic acid (0.0176 g) and 0.2 mmol of K[Au(CN)$_2$] (0.0576 g) were dissolved in a 10 mL sample bottle filled with 10 mL water. Then, this solution was exposed to 4-methoxypyrimidine vapour in a larger airtight bottle (50 mL sample bottle). Colorless crystals were obtained using this method.‡

Complexes **1Ag** and **1Ag·0.25G** were obtained as a mixture. These complexes were synthesized using Mohr's salt Fe(NH$_4$)$_2$(SO$_4$)$_2$·6H$_2$O and K[Ag(CN)$_2$] in a 1 : 2 molar ratio and 4-methoxypyrimidine. In the synthesis of the powder sample, 0.4 mmol of Mohr's salt Fe(NH$_4$)$_2$(SO$_4$)$_2$·6H$_2$O (0.1569 g) and 0.96 mmol of 4-methoxypyrimidine (0.1060 g) were dissolved in 3 mL of water (solution 1) and 0.8 mmol of K[Ag(CN)$_2$] (0.1664 g) was dissolved in 7 mL of water (solution 2). Then solution 2 was dropped into solution 1. Subsequently, 0.2079 g of white powder of **1Ag** and **1Ag·0.25G** was obtained as a mixture by this method. In the synthesis of a single crystal, 0.1 mmol of Mohr's salt Fe(NH$_4$)$_2$(SO$_4$)$_2$·6H$_2$O (0.0392 g) and 0.2 mmol of K[Ag(CN)$_2$] (0.0398 g) were dissolved in a 10 mL sample bottle filled with 10 mL water. Then this solution was exposed to 4-methoxypyrimidine vapour in a larger airtight bottle (50 mL sample bottle). Clear (**1Ag**) and orange (**1Ag·0.25G**) crystals were obtained and separated.

Complex **2Au·0.25G** was synthesized using Mohr's salt Fe(NH$_4$)$_2$(SO$_4$)$_2$·6H$_2$O, L-ascorbic acid, K[Au(CN)$_2$] and 4-methoxypyrimidine in a 1 : 1 : 2 : 2 molar ratio and excess 4,6-dimethoxypyrimidine. In the synthesis of a powder sample, 0.4 mmol (0.1590 g) of Mohr's salt, 0.4 mmol (0.0707 g) of L-ascorbic acid, excess 4,6-dimethoxypyrimidine (0.3535 g, 2.4 mmol) and 0.8 mmol (0.0881 g) of 4-methoxypyrimidine were dissolved in 6 mL of water (solution 1) and 0.8 mmol (0.2314 g) of K[Au(CN)$_2$] was dissolved in 4 mL of water (solution 2). Then solution 2 was dropped into solution 1. Subsequently, 0.2097 g (0.259 mmol, 32% yield) of white powder was obtained by this method. In the synthesis of a single crystal, 0.1 mmol (0.0392 g) of Mohr's salt, 0.1 mmol (0.0176 g) of L-ascorbic acid, 0.2 mmol (0.0576 g) of K[Au(CN)$_2$] and excess of 4,6-dimethoxypyrimidine (0.1401 g, 1.0 mmol) were dissolved in a 10 mL sample bottle filled with 10 mL water. Then this solution was exposed to 4-methoxypyrimidine vapour in a larger airtight bottle (50 mL sample bottle). A colorless crystal was obtained using this method.

Complex **2Ag·0.25G** was synthesized using Mohr's salt Fe(NH$_4$)$_2$(SO$_4$)$_2$·6H$_2$O, K[Ag(CN)$_2$] and 4-methoxypyrimidine in a 1 : 2 : 2 molar ratio and excess of 4,6-dimethoxypyrimidine. In the synthesis of the powder sample, 0.5 mmol (0.1956 g) of Mohr's salt and excess 4,6-dimethoxypyrimidine (0.2802 g, 2.0 mmol) were dissolved in 10 mL of water (solution 1) and 1.0 mmol (0.2041 g) of K[Ag(CN)$_2$] and 1.1 mmol (0.1171 g) of 4-methoxypyrimidine were dissolved in 5 mL of water (solution

‡Crystal data of complex **1Au**; $C_{14}H_{12}N_8O_2FeAu_2$, M = 774.17 g mol^{-1}, CCDC reference number: 2191439 (296 K) and 2191440 (100 K). **1Ag**; $C_{14}H_{12}N_8O_2FeAg_2$, M = 595.97 g mol^{-1}, CCDC reference number: 2191441 (296 K) and 2191442 (90 K). **1Ag·0.25G**; $C_{14}H_{12}N_8O_2FeAg_2{\cdot}0.25(C_5H_6N_2O)$, M = 623.50 g mol^{-1}, CCDC reference number: 2191443 (296 K), 2191444 (190 K), 2191445 (130 K) and 2191446 (87 K). **2Au·0.25G**; $C_{14}H_{12}N_8O_2FeAu_2{\cdot}0.25(C_6H_8N_2O_2)$, M = 809.202 g mol^{-1}, CCDC reference number: 2191447 (296 K) and 2191448 (90 K). **2Ag·0.25G**; $C_{14}H_{12}N_8O_2FeAg_2{\cdot}0.25(C_6H_8N_2O_2)$, M = 631.00 g mol^{-1}, CCDC reference number: 2191449 (296 K), 2191450 (150 K) and 2191451 (90 K)

2). Then solution 2 was dropped into solution 1. Subsequently, 0.2197 g (0.348 mmol, 35% yield) of white powder was obtained by this method. In the synthesis of a single crystal, 0.1 mmol (0.0392 g) of Mohr's salt, 0.05 mmol (0.0088 g) of L-ascorbic acid, 0.2 mmol (0.0398 g) of $K[Ag(CN)_2]$ and excess 4,6-dimethoxypyrimidine (0.1401 g, 1.0 mmol) were dissolved in a 10 mL sample bottle filled with 10 mL water. Then this solution was exposed to 4-methoxypyrimidine vapour in a larger airtight bottle (50 mL sample bottle). A colorless crystal was obtained using this method.

The expected compositions of the synthesized complexes were confirmed by elemental analysis using J-Science MICRO CORDER JM10, (**1Au**: anal. calcd for $C_{14}H_{12}N_8O_2FeAu_2$: C, 21.72%; H, 1.56%; N, 14.48%. Found: C, 21.67%; H, 1.64%; N, 14.49%, **1Ag** and **1Ag·0.25G**: anal. calcd for $C_{14}H_{12}N_8O_2FeAg_2$ (**1Ag**): C 28.21%, H 2.03%, N 18.81%. anal. calcd for $C_{14}H_{12}N_8O_2FeAg_2{\cdot}0.25(C_5H_6N_2O)$ (**1Ag·0.25G**): C 29.38%, H 2.18%, N 19.10%. Found: 28.71%, H 2.23%, N 18.94%, **2Au·0.25G**: anal. calcd for $C_{14}H_{12}N_8O_2FeAu_2{\cdot}0.25(C_6H_8N_2O_2)$: C, 23.00%; H, 1.74%; N, 14.72%. Found: C, 23.02%; H, 1.92%; N, 14.68%. **2Ag·0.25G**: anal. calcd for $C_{14}H_{12}N_8O_2FeAg_2{\cdot}0.25$ $(C_6H_8N_2O_2)$: C, 29.50%; H, 2.24%; C, 18.87%. Found: C, 29.61%; H, 2.38%; N, 18.97%). This complex was identified by TG analysis using a Hitachi High-Technologies Corporation TG/DTA6200 (Fig. S1–S4†) and powder X-ray diffraction measurement using a Rigaku Co. X-ray diffractometer or MAC Science M03XHF22 (Fig. S5–S8†). The presence of **1Ag** in the **1Ag·0.25G** powder was confirmed *via* powder X-ray diffraction measurement (Fig. S6†).

The superconducting quantum interference device (SQUID) method from Quantum Design MPMS - 5S was used to measure the magnetic susceptibility of the complexes in the temperature range of room temperature to 4 K under a 0.1 T field and a cooling rate of 1 K min^{-1}. The sample used for measurement was filled in a gelatine capsule, which was filled with a plastic straw. The magnetic susceptibility of **1Ag** was measured using a pure single crystal, while that of the other samples was measured using a powder sample. We measured the magnetic susceptibility of the powder sample of **1Ag·0.25G** twice, where the repeated measurement result is shown in Fig. S13;† however, we could not measure this property of the pure crystal of **1Ag·0.25G** due to the worldwide helium shortage.

The crystal structure of the synthesized complexes was determined by single-crystal X-ray diffraction (XRD) using a Bruker SMART diffractometer having a Mo-Kα line at 298 K (HS state), 190 K (intermediate state), and 150 K (LS state). The structure was solved using the SHELX 2014 software.[24,25]

Results and discussion

Fig. 1 and 2 show the magnetic susceptibilities of **1Au**, **1Ag**, **1Ag·0.25G**, and **2Au·0.25G**. Comparing these complexes, **1Au** and **1Ag** did not demonstrate the SCO phenomenon. **1Ag·0.25G** showed a three-step spin transition between 70 and

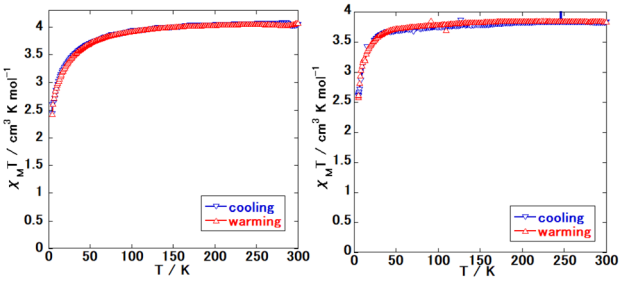

Fig. 1 Magnetic susceptibility of the synthesized complex. (Left: **1Au** and right: **1Ag** (pure crystal).)

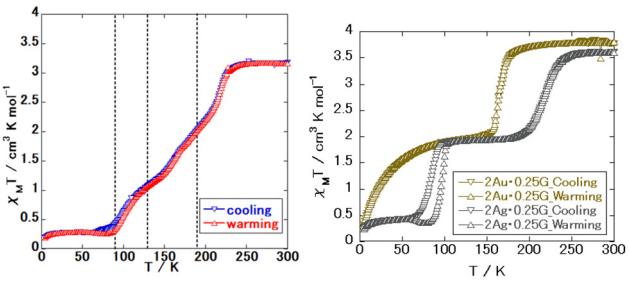

Fig. 2 Magnetic susceptibility of guest-clathrate complex. (Left: **1Ag·0.25G** (powder) and right: **2Au·0.25G** and **2Ag·0.25G**.)

250 K, where the 1st step is abrupt, and 2nd and 3rd steps are gradual. **2Au·0.25G** showed an abrupt one-step spin transition between 150 and 180 K, and half the magnetic susceptibility, **2Ag·0.25G** showed a relatively gradual one-step spin transition between 180 and 260 K and its magnetic susceptibility was halved. These results suggest that **1Au** and **1Ag** do not exhibit the SCO phenomenon, and all the Fe sites show the HS state below room temperature. The other samples showed the SCO phenomenon, where all the Fe sites in complex **1Ag·0.25G** changed to the LS state, while only half of the Fe site in complex **2Au·0.25G** changed to the LS state. In the case of **1Au**, its magnetic susceptibility is ~4 cm^3 mol K^{-1} above 100 K, while that of **1Ag** is ~3.8 cm^3 mol K^{-1} above 100 K. These values are higher than the calculated spin only octahedral magnetic susceptibility of the high spin Fe site (S = 2) of ~3.0 cm^3 mol K^{-1}, which can be explained by the spin–orbital coupling.

In the case of **1Ag·0.25G**, its magnetic susceptibility at 298 K was 3.15 cm^3 mol K^{-1}, at 190 K it was 2.03 cm^3 mol K^{-1}, at 130 K it was 1.13 cm^3 mol K^{-1}, and at 50 K it was 0.28 cm^3 mol K^{-1}. This shows that this complex has all four states, *i.e.*, all HS, ~2/3 HS, ~1/3 HS, and all LS states. For **2Au·0.25G**, its magnetic susceptibility at 298 K was 3.77 cm^3 mol K^{-1}, while that at 140 K is 1.99 cm^3 mol K^{-1}. This shows this complex has two spin states, *i.e.*, all HS and 1/2 HS. In the case of **2Ag·0.25G**, its magnetic susceptibility at 298 K is 3.6 cm^3 mol K^{-1}, at 150 K, it was 1.94 cm^3 mol K^{-1}, and at 50 K it was 0.43 cm^3 mol K^{-1}. This shows three spin states, *i.e.*, all HS and

1/2 HS states, which are similar to that of **2Au·0.25G**, and all the LS states may exist below 50 K.

Fig. 3 and 4 show the crystal structure of **1Au** and **1Ag**, respectively. These complexes show a single-layer Soma–Iwamoto type structure without aurophilic or argentophilic interaction. The space group of both complexes was determined to be $P2_1/n$ at RT and low temperature. The detailed crystallographic data is available in Tables S1–S4.† Comparing the RT and low temperature data, no bond length change was observed (Table 1). The insignificant change in the crystal structure between RT and low temperature supports that **1Au** and pure **1Ag** do not show the SCO phenomenon by magnetic measurements.

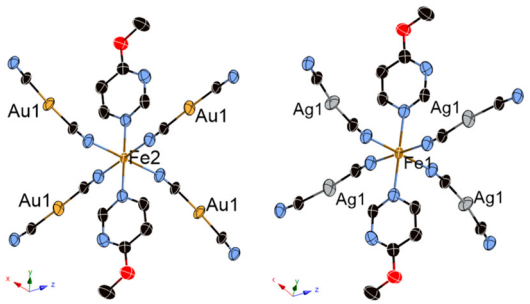

Fig. 3 ORTEP structures of **1Au** and **1Ag**. (Left: **1Au** and right: **1Ag**.)

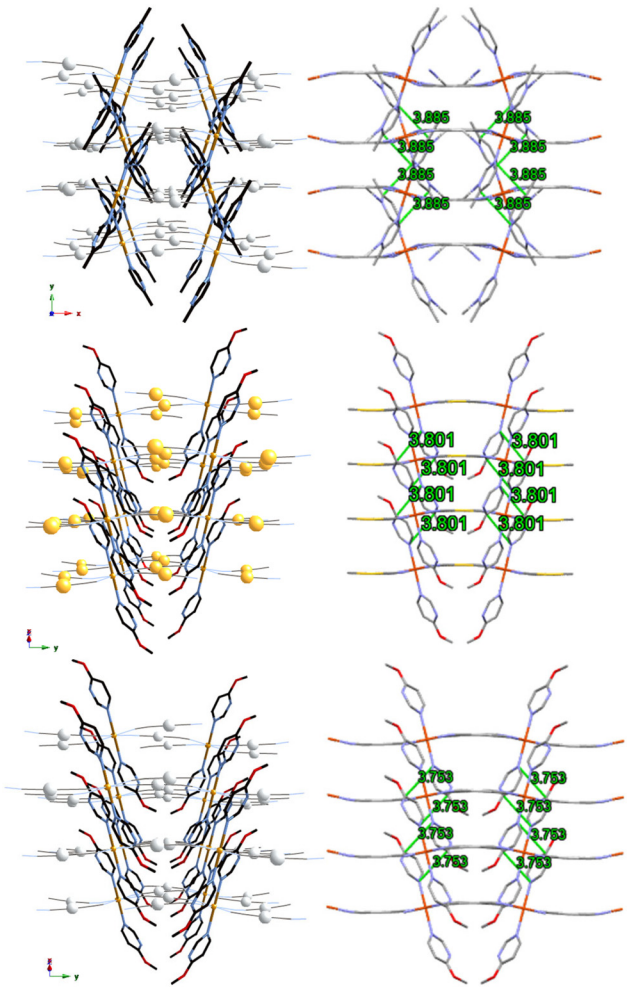

Fig. 4 Packing structure of {Fe(4-methylpyrimidine)$_2$[Ag(CN)$_2$]$_2$}[16] (top, along the *c* axis), **1Au** (middle, along the [1 0 −1] axis) and **1Ag** (bottom, along the [1 0 −1] axis). (Gray: C, blue: N, red: N, orange: Fe, silver: Ag, yellow: Au.)

The Ag–N$_{ligand}$ distance in **1Ag** is closer than the Au–N$_{ligand}$ distance in **1Au** by more than 0.3 Å (Table 1). This means that the Ag–N interaction is slightly stronger than the Au–N interaction. This can be explained by the relativistic effect.[16,23] Furthermore, this trend was observed in previously reported Au- and Ag-type complexes using 4-methylpyrimidine.[15,16]

Comparing **1Au** and **1Ag** with {Fe(4-methylpyrimidine)$_2$[Au(CN)$_2$]$_2$}[15] and {Fe(4-methylpyrimidine)$_2$[Ag(CN)$_2$]$_2$},[16] respectively, **1Au** shows a single-layered Soma–Iwamoto-type structure without Au–Au interaction, while {Fe(4-methylpyrimidine)$_2$[Au(CN)$_2$]$_2$} shows a double-layered Soma–Iwamoto-type structure with Au–Au interaction. Also, **1Ag** does not show the SCO phenomenon, while {Fe(4-methylpyrimidine)$_2$[Ag(CN)$_2$]$_2$} shows the SCO phenomenon even though both complexes possess a Soma–Iwamoto-type single layer with Ag–N interaction. This result can be explained by the difference in the coordination field due to the different π–π interactions (Table 2) and electron density. The former difference led to a difference in the stacking of the pyrimidine ligands. The stacking of the pyrimidine ligands of **1Au** and **1Ag** were alternately arranged in a V-shape, whereas that of {Fe(4-methylpyrimidine)$_2$[Ag(CN)$_2$]$_2$} crossed and arranged in an X-shape (Fig. 4). The latter difference can be explained by the greater electron-donating ability of the methoxy group compared to that of the methyl group. This led to the greater electron density and lower electrophilicity of 4-methoxypyrimidine than that of 4-methylpyrimidine, and thus 4-methoxypyrimidine forms a weaker coordination field than 4-methylpyrimidine. Consequently, **1Au** and **1Ag** show the HS state even at very low temperatures.

Fig. 5 shows the crystal structure of **1Ag·0.25G**, which shows a double-layered penetrated Hofmann-type structure with five Fe sites. At 296 K, the layers intersect at an angle of 39.89°. Layer 1 consists of two nonequivalent Fe sites at a ratio of 1 : 1. In contrast, layer 2 contains three non-equivalent Fe sites at a

Table 1 Bond lengths of complexes **1Au** and **1Ag**

Average bond lengths/Å				
	1Au (M = Au)		**1Ag** (M = Ag)	
T/K	296(2)	100(2)	296(2)	90(2)
Fe–N$_{ligand}$	2.229(3)	2.223(3)	2.241(2)	2.2363(14)
Fe–N$_{cyano}$	2.159(3)	2.155(3)	2.1579(19)	2.1532(14)
M–C	1.976(4)	1.983(3)	2.059(2)	2.0613(17)
M–N$_{ligand}$	3.435	3.373	3.125	2.988
M–M	4.780	4.658	4.729	4.604

Table 2 π–π interaction distance of {Fe(4-methylpyrimidine)$_2$[Ag(CN)$_2$]$_2$},[16] **1Au** and **1Ag**

π–π interaction distance/Å				
		Ref. 16	**1Au**	**1Ag**
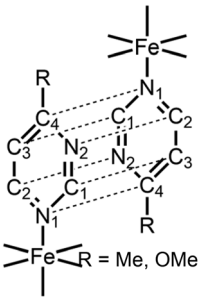	N_1–C_4	3.885	3.801	3.753
	N_2–C_2	3.804	3.754	3.691
	C_1–C_3	3.833	3.754	3.671

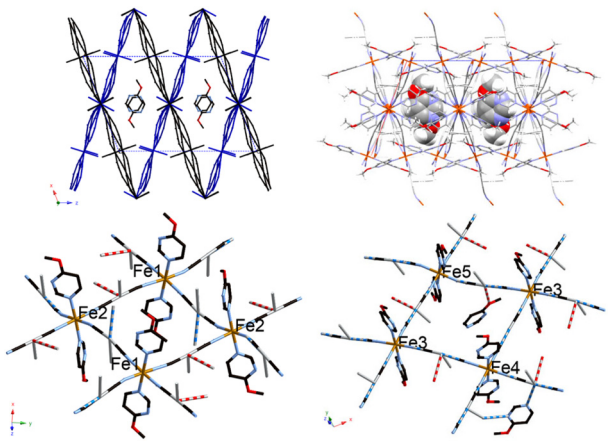

Fig. 5 Structure of **1Ag·0.25G**. (Upper left: packing structure along the *Y* axis (ligand molecules are omitted), upper right: space filling of guest molecule, lower left: structure of layer 1, and lower right: structure of layer 2.)

ratio of 2 : 1 : 1. Layers 1 and 2 are along the (1 0 0) and (−1 0 2) planes of the unit lattice, respectively. Additionally, an Ag–Ag interaction exists between layers 1 and 2. The space group was determined to be $P2_1/c$ at 296 K, 190 K, 130 K and 87 K. The detailed crystallographic data is available in Tables S5–S8.† Table 3 shows the bond length of **1Ag·0.25G**, which indicates that an argentophilic interaction exists between the two layers. At 190 K, half of the Fe site on layer 1 transforms to the LS state, and a quarter of that on layer 2 transforms to the LS state. Consequently, five-eighths of the Fe site remains in the HS state at 190 K. At 87 K, all of the Fe site on layer 1 is transformed to the LS state, while half of that on layer 2 is transformed to the LS state. Therefore, a quarter of the Fe site remains in the HS state at 87 K. Thus, **1Ag·0.25G** shows three spin states, *i.e.*, HS, $HS_{5/8}LS_{3/8}$, and $HS_{1/4}LS_{3/4}$ (Fig. 6). This result supports the multi-step SCO phenomenon in magnetic susceptibility. The two non-equivalent Soma–Iwamoto-type layers can explain this phenomenon. Also, **1Ag·0.25G** may show completely spin transition states, *e.g.*, all LS states, at very low temperatures due to its almost zero magnetic susceptibility at very low temperatures. Its crystal structure at 130 K is similar to that at 87 K even though the powder sample showed a complete transition to the LS at 87 K and this behaviour was reproduced by repeating the measurement (Fig. S13†). This suggests that the spin transition temperature of the single crystal is lower than that of the powder sample. An Ag–O interaction was also observed in **1Ag·0.25G**, which can be stabilized in this structure. Penetrated structures are very interesting given that only a few Soma–Iwamoto-type complexes with penetrated structures have been reported. One of the examples of a penetrated Soma–Iwamoto-type structure is Mn(4-methylpyridine)$_2$[Ag(CN)$_2$]$_2$.[22] In contrast to the results of the Ag-type complex, the penetrated Au-type complex, *i.e.*, complex **1Au·0.25G**, was not obtained. This can be explained by the fact that the Au–N interaction is not strong enough to stabilize the penetrated structure. Comparing **1Ag·0.25G** to **1Ag**, many differences exist. That can mainly be explained by the fact that the O atoms in the methoxy group weakly coordinate to the Ag atom in the cyanometallate. This not only leads to the formation of a penetrated structure but also less electron density on 4-methoxypyrimidine than that of the non-coordinated one, creating a stronger coordination field. Thus, **1Ag·0.25G** shows the SCO phenomenon, whereas **1Ag** does not.

Fig. 7 shows the crystal structure of **2Au·0.25G**, possessing a two-layered penetrated Soma–Iwamoto-type structure with two

Table 3 Bond lengths of complex **1Ag·0.25G**

Average bond lengths/Å				
T/K	296(2)	190(2)	130(2)	87(2)
Fe–N_{ligand}	Layer 1: 2.210(10)	Layer 1: 2.223(9), 2.015(9)	Layer 1: 2.012(9)	Layer 1: 2.008(8)
	Layer 2: 2.220(10)	Layer 2: 2.198(9), 2.022(9)	Layer 2: 2.210(9), 2.005(9)	Layer 2: 2.190(9), 2.003(8)
Fe–N_{cyano}	Layer 1: 2.134(8)	Layer 1: 2.146(8), 1.948(8)	Layer 1: 1.952(8)	Layer 1: 1.944(8)
	Layer 2: 2.155(7)	Layer 2: 2.140(8), 1.943(8)	Layer 2: 2.163(7), 1.940(7)	Layer 2: 2.145(7), 1.941(7)
Ag–C	Layer 1: 2.072(10)	Layer 1: 2.070(10)	Layer 1: 2.073(9)	Layer 1: 2.068(9)
	Layer 2: 2.055(9)	Layer 2: 2.067(10)	Layer 2: 2.072(9)	Layer 2: 2.068(9)
Ag–N_{guest}	Layer 1: 3.181	Layer 1: 2.984	Layer 1: 3.012	Layer 1: 2.968
	Layer 2: 3.186	Layer 2: 3.053	Layer 2: 2.963	Layer 2: 2.944
Ag–O_{guest}	Layer 2: 3.041	Layer 2: 2.946	Layer 2: 2.902	Layer 2: 2.874
Ag–Ag	3.1154(16)	3.0832(14)	3.0783(18)	3.0599(11)

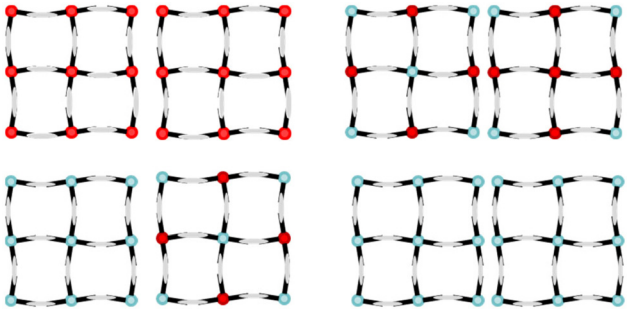

Fig. 6 Soma–Iwamoto-type layer model of **1Ag·0.25G**. (Upper left: RT, upper right: 190 K, lower left: 130 and 87 K, and lower right: lower temperature (predicted).)

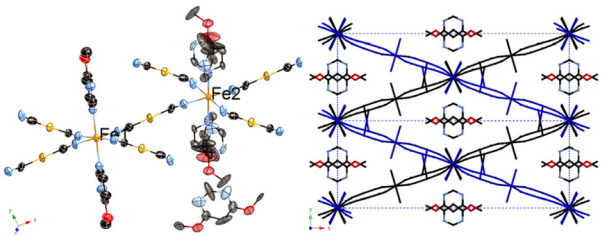

Fig. 7 Structure of **2Au·0.25G**. (Left: ORTEP structure and right: packing structure along the *Z* axis (ligand molecules are omitted).)

Fe sites ion a 1 : 1 ratio. These layers intersect at an angle of 41.14°. The Soma–Iwamoto-type layers are along two directions, *i.e.*, (1 1 0) and (−1 1 0) planes of the unit lattice. Also, an Au–Au interaction exists between the two layers. The space group was determined to be *C*2/*c* at 296 K and 100 K. The detailed crystallographic data is available in Tables S9 and S10.† Table 4 shows the bond lengths of **2Au·0.25G**, which indicate that an aurophilic interaction exists between the two layers. At 90 K, half of the Fe site remains in the HS state, and thus **2Au·0.25G** shows two spin states, *i.e.*, HS and $HS_{0.5}LS_{0.5}$ (Fig. 8). This corresponds to the magnetic measurement. The half-spin transition state was also observed in a previously reported complex, *i.e.*, {Fe(4-methylpyrimidine)$_2$[Au(CN)$_2$]$_2$}. The half-spin transition state is widely observed in complex **2Au·0.25G** at a lower temperature range. In contrast, the half-spin transition state in {Fe(4-methylpyrimidine)$_2$[Au(CN)$_2$]$_2$} is simply an intermediate state and was observed in a narrow temperature range. This can be explained by the fact that **2Au·0.25G** contains two different types of Fe sites at all temperature ranges, whereas {Fe(4-methylpyrimidine)$_2$[Au(CN)$_2$]$_2$} contains only one type of Fe site except in the intermediate state area. Also, the pyrimidine ligands coordinated to the Fe2 sites are disordered in two positions by a 0.522(13) : 0.478(13) rate. These positions are vertical, and only one position has a clathrate guest molecule. The result that not all the Fe2 sites face the same direction can be explained by the fact that the steric hindrance of the two methyl groups prevents the pyrimidine ligands from facing the same direction (Fig. 9).

In the case of **2Au·0.25G**, the 4,6-dimethoxypyrimidine guest is parallel to the 4-methoxypyrimidine ligand. That

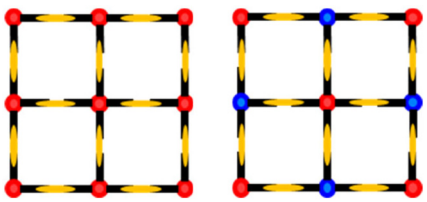

Fig. 8 Soma–Iwamoto-type layer model of **2Au·0.25G**. (Left: RT and right: 90 K.)

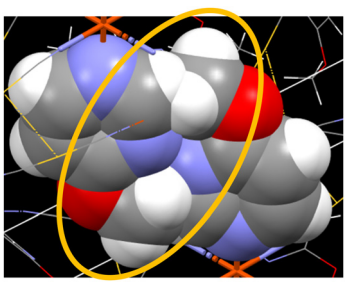

Fig. 9 Steric hindrance of the two methyl groups in **2Au·0.25G**.

Table 4 Bond lengths of complexes **2Au·0.25G** and **2Ag·0.25G**

Average bond lengths/Å

	2Au·0.25G (M = Au)		**2Ag·0.25G** (M = Ag)		
T/K	296(2)	90(2)	296(2)	150(2)	90(2)
Fe–N_{ligand}	Fe1: 2.199(11)	Fe1: 2.208(10)	Fe1: 2.237(6)	Fe1: 2.235(4)	Fe1: 2.209(9)
	Fe2: 2.20(4)	Fe2: 2.006(10)	Fe2: 2.204(8)	Fe2: 2.007(5)	Fe2: 1.998(9)
Fe–N_{cyano}	Fe1: 2.160(9)	Fe1: 2.159(11)	Fe1: 2.149(5)	Fe1: 2.144(5)	Fe1: 2.134(10)
	Fe2: 2.160(10)	Fe2: 1.934(12)	Fe2: 2.133(6)	Fe2: 1.936(5)	Fe2: 1.929(10)
M–C	1.985(13)	1.984(14)	2.058(5)	2.054(6)	1.984(14)
M–N_{guest}	3.750	3.549	3.697	3.496	3.475
M–O_{guest}	3.466	3.329	3.331	3.252	3.213
M–M	3.2056(7)	3.1291(9)	3.1569(11)	3.0940(9)	3.0807(13)

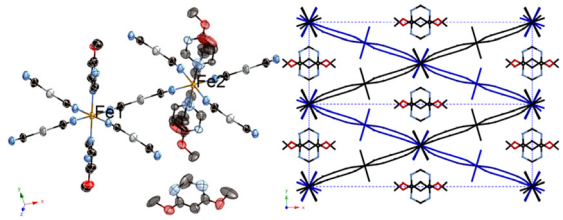

Fig. 10 Structure of **2Ag·0.25G**. (Left: ORTEP structure and right: packing structure along the *Z* axis (ligand molecules are omitted).)

suggests that a π–π interaction exists between the host structure and guest molecule.

Fig. 10 shows the crystal structure of **2Ag·0.25G**, where the pyrimidine ligands coordinated to Fe2 atoms are disordered to two positions and isostructural to **2Au·0.25G** by a 0.482(7) : 0.518(7) rate, and Table 4 also shows the bond lengths of **2Ag·0.25G**. The results indicate that an argentophilic interaction occurs between the two layers, and the Soma–Iwamoto-type layers intersect at an angle of 43.23°. The Soma–Iwamoto-type layers are along two directions, *i.e.*, the (1 1 0) and (−1 1 0) planes of the unit lattice. At 150 and 90 K, half of the Fe site remains in the HS state, and thus **2Ag·0.25G** shows two spin states, *i.e.*, HS and $HS_{0.5}LS_{0.5}$ (Fig. 11). This corresponds to the magnetic measurement. Also, **2Ag·0.25G** may show complete spin transition states, *e.g.*, all LS states, at very low temperatures due to its almost zero magnetic susceptibility at very low temperatures. The space group was determined to be *C*2/*c* at 296, 150 and 90 K. The detailed crystallographic data is available in Tables S11–S13.† In the unit cell of complex **2Ag·0.25G**, β is very close to 90°. However, this is monoclinic given that no symmetry elements on the *a* and *c* axis were detected by the ADDSYM search in PLATON.

Comparing **2Au·0.25G** and **2Ag·0.25G**, the Ag–N distance in **2Ag·0.25G** is closer than the Au–N distance in **2Au·0.25G** by less than 0.16 Å, which is a smaller difference than the non-guest-type structure. The shorter M–N distance suggests that the more electron-deficient pyrimidine ring has a stronger coordination interaction of the pyrimidine N atom to Ag or Au atom in the bridging ligand. That leads to a stronger coordination field. In fact, **2Ag·0.25G** showed a higher transition temperature than **2Au·0.25G**, and additionally all LS state by magnetic measurement.

Due to the limitation of the cryostat, it was impossible to observe all the LS states in **1Ag·0.25G** and **2Ag·0.25G** at very low temperatures using single-crystal XRD measurement.

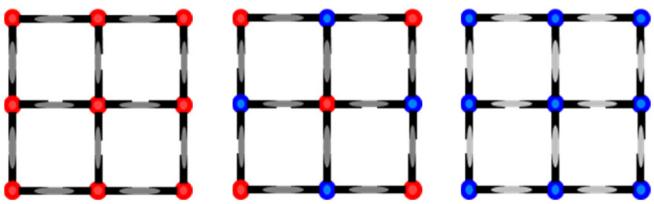

Fig. 11 Soma–Iwamoto-type layer model of **2Ag·0.25G**. (Left: RT, center: 150 and 90 K, and right: low temperature (predicted).)

Comparing the non-guest complexes, **1Au** and **1Ag**, and the guest clathrate complexes, **1Ag·0.25G** and **2Au·0.25G**, respectively, **2Ag·0.25G**. **1Au** and **1Ag** show normal Soma–Iwamoto-type structures, whereas the other is penetrated. This behaviour is similar to the case of $[Cd(py)_2\{Ag(CN)_2\}_2]$ and $[Cd(py)_2\{Ag(CN)_2\}_2]$·Guest (Guest = benzene or pyrrole), where the former shows a single-layered Soma–Iwamoto-type structure, while the latter shows a penetrated structure.

The crystals of **1Ag·0.25G**, **2Au·0.25G**, and **2Ag·0.25G** were obtained as twin crystals. The twin matrix is shown in Fig. 12.

These complexes can be easily twinned as another layer grows beyond one layer with little lattice misalignment due to twinning.

In **1Ag·0.25G**, the angle formed by the (−1 0 2) plane and (0 0 1) plane is near to 180° − β (69.346(2)°), and thus this complex can be twinned by the (−1 0 2) plane (Fig. 13).

In **2Ag·0.25G** and **2Au·0.25G**, the β angle of these complexes is close to 90°, and thus their single crystals can be easily twinned by the (1 0 0) or (0 0 1) plane.

Comparing **1Ag·0.25G** with **2Ag·0.25G** (and **2Au·0.25G**), it was observed that the former complex has two inequivalent layers and gradual three-step SCO phenomenon, whereas the

$$\mathbf{1Ag\cdot 0.25G}\begin{pmatrix}-1 & 0 & 0.5\\ 0 & -1 & 0\\ 0 & 0 & 1\end{pmatrix} \qquad \begin{matrix}\mathbf{2Au\cdot 0.25G}\\ \mathbf{2Ag\cdot 0.25G}\end{matrix}\begin{pmatrix}-1 & 0 & 0\\ 0 & -1 & 0\\ 0 & 0 & 1\end{pmatrix}$$

Fig. 12 Twin matrix of **1Ag·0.25G**, **2Au·0.25G**, and **2Ag·0.25G**.

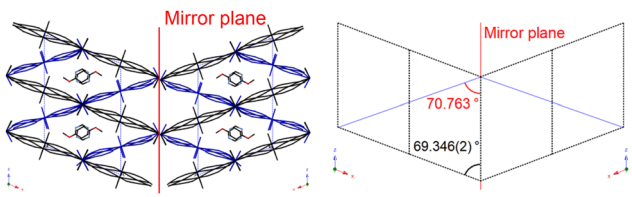

Fig. 13 Twinning effect of **1Ag·0.25G**.

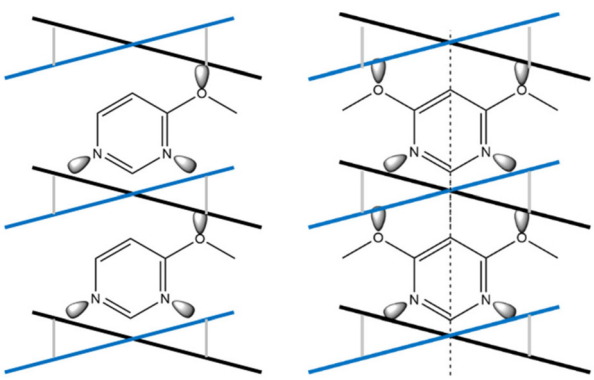

Fig. 14 Comparison of the symmetry of the penetrated Soma–Iwamoto-type layer and guest molecule between **1Ag·0.25G** and **2Au·0.25G**.

latter complex contains two equivalent layers and one- or two-step SCO phenomenon. This difference can be explained by the symmetry of the guest molecule (Fig. 14). In **1Ag·0.25G**, 4-methoxypyrimidine does not have a mirror plane orthogonal to the pyrimidine ring, and thus the two Soma–Iwamoto-type layers of **1Ag·0.25G** are inequivalent. In contrast, that of **2Ag·0.25G** is equivalent because 4,6-dimethoxypyrimidine has a mirror plane orthogonal to the pyrimidine ring. This leads to a difference in the number of inequivalent Fe sites and intermediate states.

In the 4,6-dimethoxyprrimidine clathrate complex, *i.e.*, **2Au·0.25G** and **2Ag·0.25G**, a penetrated structure was not only observed in the Ag-type complex but also the Au-type complex, where the two methoxy groups can explain the additional M–O interaction.

Conclusions

Using the 4-methoxypyrimidine ligand, **1Au**, **1Ag**, **1Ag·0.25G**, **2Au·0.25G**, and **2Ag·0.25G**, we synthesized a novel Soma–Iwamoto-type complex. We showed *via* magnetic susceptibility that **1Ag·0.25G** and **2Au·0.25G** exhibit the SCO phenomenon. **1Ag·0.25G** exhibits a gradual three-step SCO phenomenon, **2Au·0.25G** exhibits an abrupt one-step half SCO phenomenon, and **2Ag·0.25G** exhibits an abrupt two-step SCO phenomenon. In the crystal structure of all the synthesized complexes, Ag–N or Au–N interaction exists. Moreover, **1Au** and **1Ag** are isostructural as well as **2Au·0.25G** and **2Ag·0.25G**. **1Au** and **1Ag** show only the HS state. **1Ag·0.25G** shows three spin states, *i.e.*, HS, $HS_{5/8}LS_{3/8}$, and $HS_{1/4}LS_{3/4}$. **2Au·0.25G** and **2Ag·0.25G** show two spin states, *i.e.*, HS and $HS_{1/2}LS_{1/2}$. **1Ag·0.25G** and **2Ag·0.25G** exhibit all the LS states at very low temperatures. Complexes **1Ag·0.25G**, **2Au·0.25G**, and **2Ag·0.25G** show penetrated Soma–Iwamoto-type structures, which are interesting given that only a few of these structures has been reported to date. Comparing the Ag-type complex **1Ag** and **2Ag·0.25G** and Au-type complex **2Au** and **2Au·0.25G**, the Ag–N distance is closer than the Au–N distance. This can be explained by the fact that the Ag–N interaction is stronger than the Au–N interaction.

Conflicts of interest

There are no conflicts to declare.

References

1 K. A. Hofmann and F. Z. Küspert, Verbindungen von Kohlenwasserstoffen mit Metallsalzen, *Z. Anorg. Allg. Chem.*, 1897, **15**, 204.
2 T. Kitazawa, Y. Gomi, M. Takahashi, M. Takeda, M. Enomoto, A. Miyazaki and T. Enoki, Spin-crossover behaviour of the coordination polymer FeII(C5H5N)2NiII(CN)2, *J. Mater. Chem.*, 1996, **6**, 119.
3 V. M. Hiiuk, S. Shova, A. Rotaru, A. A. Golub, I. O. Fritsky and I. A. Gural'skiy, Spin crossover in 2D iron(II) phthalazine cyanometallic complexes, *Dalton Trans.*, 2020, **49**, 5302–5311.
4 L. Piñeiro-López, M. Seredyuk, M. C. Muñoz and J. A. Real, Effect of Guest Molecules on Spin Transition Temperature in Loaded Hofmann-Like Clathrates with Improved Porosity, *Eur. J. Inorg. Chem.*, 2020, 764–769.
5 R. Li, G. Levchenko, F. J. Valverde-Muñoz, A. B. Gaspar, V. V. Ivashko, Q. Li, B. Liu, M. Yuan, H. Fylymonov and J. A. Real, Pressure Tunable Electronic Bistability in Fe(II) Hofmann-like Two-Dimensional Coordination Polymer [Fe(Fpz)2Pt(CN)4]: A Comprehensive Experimental and Theoretical Study, *Inorg. Chem.*, 2021, **60**, 16016–16028.
6 F. J. Valverde-Muñoz, R. Kazan, K. Boukheddaden, M. Ohba, J. A. Real and T. Delgado, Downsizing of Nanocrystals While Retaining Bistable Spin Crossover Properties in Three-Dimensional Hofmann-Type {Fe(pz)[Pt(CN)$_4$]}$^-$ Iodine Adducts, *Inorg. Chem.*, 2021, **60**, 8851–8860.
7 I. S. Kuzevanova, O. I. Kucheriv, V. M. Hiiuk, D. D. Naumova, S. Shova, S. I. Shylin, V. Kotsyubynsky, A. Rotaru, I. O. Fritsky and I. A. Gural'skiy, Spin crossover in iron(II) Hofmann clathrates analogues with 1,2,3-triazole, *Dalton Trans.*, 2021, **50**, 9250–9258.
8 D. J. Mondal, A. Mondal, A. Paul and S. Konar, Guest-Induced Multistep-to-One-Step Reversible Spin Transition with Enhanced Hysteresis in a 2D Hofmann Framework, *Inorg. Chem.*, 2022, **61**, 4572–4580.
9 T. Kosone, R. Kosuge, M. Tanaka, T. Kawasaki and N. Adachi, New family of Hofmann-like coordination polymers constructed with imidazole ligands and associated with spin crossover and anisotropic thermal expansions, *New J. Chem.*, 2022, **46**, 10540–10544.
10 V. Niel, J. M. Martínez-Agudo, M. C. Muñoz, A. B. Gaspar and J. A. Real, Cooperative Spin Crossover Behavior in Cyanide-Bridged Fe(II)–M(II) Bimetallic 3D Hofmann-like Networks (M = Ni, Pd, and Pt), *Inorg. Chem.*, 2001, **40**, 3838–3839.
11 Y.-Y. Peng, S.-G. Wu, Y.-C. Chen, W. Liu, G.-Z. Huang, Z.-P. Ni and M.-L. Tong, Asymmetric seven-/eight-step spin-crossover in a three-dimensional Hofmann-type metal–organic framework, *Inorg. Chem. Front.*, 2020, **7**, 1685–1690.
12 K.-P. Xie, Z.-Y. Ruan, X.-X. Chen, J. Yang, S.-G. Wu, Z.-P. Ni and M.-L. Tong, Light-induced hidden multistability in a spin crossover metal–organic framework, *Inorg. Chem. Front.*, 2022, **9**, 1770–1776.
13 V. M. Hiiuk, S. I. Shylin, D. D. Barakhtii, D. M. Korytko, V. O. Kotsyubynsky, A. Rotaru, S. Shova and I. A. Gural'skiy, Two-Step Spin Crossover in Hofmann-Type Coordination Polymers [Fe(2-phenylpyrazine)2{M(CN)2}2] (M = Ag, Au), *Inorg. Chem.*, 2022, **61**, 2093–2104.
14 S. Wu, S. Bala, Z. Ruan, G. Huang, Z. Ni and M. Tong, Four-step spin-crossover in an oxamide-decorated metal-organic framework, *Chin. Chem. Lett.*, 2022, **33**, 1381–1384.
15 K. Kitase and T. Kitazawa, A novel two-step Fe–Au type spin-crossover behavior in a Hofmann-type coordination

complex {Fe(4-methylpyrimidine)$_2$[Au(CN)$_2$]$_2$}, *Dalton Trans.*, 2020, **49**, 12210–12214.

16 K. Kitase, D. Akahoshi and T. Kitazawa, Effects of both methyl and pyrimidine groups in Fe–Ag spin-crossover Hofmann-type complex {Fe(4-methylpyrimidine)2[Ag(CN)2]2}, *Inorg. Chem.*, 2021, **60**, 4717–4722.

17 T. Soma, H. Yuge and T. Iwamoto, Three-Dimensional Interpenetrating Double and Triple Framework Structures in [Cd(bpy)$_2${Ag(CN)$_2$}$_2$] and [Cd(pyrz){Ag$_2$(CN)$_3$}{Ag(CN)$_2$}], *Angew. Chem., Int. Ed. Engl.*, 1994, **33**, 1665–1666.

18 T. Soma and T. Iwamoto, Variations of multi-dimensional supramolecular structures built of the two-dimensional [Cd(py)$_2${Ag(CN)$_2$}$_2$]$_n$ network: Three-dimensional textile structures of catena-poly[trans-bis(pyridine)cadmium(II)-di-μ-{dicyanoargentato(I)-N,N′}·G (G = benzene or pyrrole) and two-dimensional layer structure of catena-poly[trans-bis(pyridine)cadmium(II)-di-μ-{dicyanoargentato(I)-N,N′}], *J. Inclusion Phenom. Macrocyclic Chem.*, 1996, **26**, 161–173.

19 S. Nishikiori, T. Soma and T. Iwamoto, In-plane and Out-of-plane Motion of Benzene Trapped in a Cd(py)$_2${Ag(CN)$_2$}$_2$ Host as Studied by Deuterium NMR, *J. Inclusion Phenom. Macrocyclic Chem.*, 1997, **27**, 233–243.

20 J. A. Rodriguez-Velamazán, M. Castro, E. Palacios, R. Burriel, T. Kitazawa; and T. Kawasaki, A Two-Step Spin Transition with a Disordered Intermediate State in a New Two-Dimensional Coordination Polymer, *J. Phys. Chem. B*, 2007, **111**, 1256–1261.

21 T. Kosone, C. Kachi-Terajima, C. Kanadani, T. Saito and T. Kitazawa, Isotope Effect on Spin-crossover Transition in a New Two-dimensional Coordination Polymer [Fe^{II}(C$_5$H$_5$N)$_2$][Au^{I}(CN)$_2$]$_2$, [FeII(C5D5N)2][AuI(CN)2]2, and [FeII(C5H515N)2][AuI(CN)2]2, *Chem. Lett.*, 2008, **37**, 754–755.

22 T. Kosone, Y. Suzuki, C. Kanadani, T. Saito and T. Kitazawa, Structural Isomers of {MnII(L)2[AgI(CN)2]2} (L = 3-Methylpyridine or 4-Methylpyridine), Bilayer Structure with Binuclear Argentophilic Interaction and Interpenetrated Structure with 1D Chain Argentophilic Interaction; Synthesis, Crystal Structure, and Magnetic Properties, *Bull. Chem. Soc. Jpn.*, 2009, **82**(3), 347–351.

23 P. Pyykkö, *Chem. Rev.*, 1988, **88**, 563–594.

24 G. M. Sheldrick, *Acta Crystallogr., Sect. C: Struct. Chem.*, 2015, **71**, 3–8.

25 G. M. Sheldrick, *Acta Crystallogr., Sect. A: Found. Crystallogr.*, 2008, **64**, 112–122.